

Oscillations and instabilities of fast and differentially rotating relativistic stars

Christian Krüger,¹ Erich Gaertig,¹ and Kostas D. Kokkotas^{1,2}

¹*Theoretical Astrophysics, Eberhard-Karls University of Tübingen, Tübingen 72076, Germany*

²*Department of Physics, Aristotle University of Thessaloniki, Thessaloniki 54124, Greece*

(Dated: October 28, 2018)

We study non-axisymmetric oscillations of rapidly and differentially rotating relativistic stars in the Cowling approximation. Our equilibrium models are sequences of relativistic polytropes, where the differential rotation is described by the relativistic j -constant law. We show that a small degree of differential rotation raises the critical rotation value for which the quadrupolar f -mode becomes prone to the CFS instability, while the critical value of $T/|W|$ at the mass-shedding limit is raised even more. For stiffer equations of state these effects are even more pronounced. When increasing differential rotation further to a high degree, the neutral point of the CFS instability first reaches a local maximum and is lowered afterwards. For stars with a rather high compactness we find that for a large degree of differential rotation the absolute value of the critical $T/|W|$ is below the corresponding value for rigid rotation. We conclude that the onset of the CFS instability is eased for a small degree of differential rotation and for a large degree at least in stars with a higher compactness. Moreover, we were able to extract the eigenfrequencies and the eigenfunctions of r -modes for differentially rotating stars and our simulations show a good qualitative agreement with previous Newtonian results.

PACS numbers: 04.30.Db, 04.40.Dg, 95.30.Sf, 97.10.Sj

I. INTRODUCTION

Rapidly spinning neutron stars can be destabilized due to the CFS [1–3] instability. This instability, for quadrupole non-axisymmetric perturbations with $m = 2$, sets in for uniformly rotating polytropes when $\beta = T/|W| \approx 0.14$ where T is the rotational kinetic energy and W is the gravitational potential energy of the star. For higher values of m the instability sets in for smaller rotational rates but the growth time is considerable longer and viscosity stabilizes the star. The CFS instability is generic for r -modes, i. e. these modes are CFS unstable for any rotational rate while for the f -modes the previous value of β is approximately correct. This value of β corresponds to rotational frequencies of the stars which are 85-90% of the Kepler frequency. These high spin frequencies have not yet been observed in nature but it is expected that they may be met in newly born neutron stars. Newly born neutron stars are expected to rotate not only fast but also differentially, and this is a factor that has to be taken into account in the study of instabilities.

Actually, differential rotation can appear in many phases of the stellar evolution of a neutron star, such as in proton-neutron stars [4, 5], in the massive remnant of binary neutron star mergers [6–8], or as a result of stellar oscillations (r -modes) that may drive the star into differential rotation via nonlinear effects [9–12]. The phase where the star rotates differentially can last between seconds to months, depending on the dissipative mechanism that drive the star to uniform rotation, such as viscosity, magnetic braking [13, 14] and turbulent motion [15, 16]. However, this very short period is met during the most violent phases of neutron star's life, as in the case of a core collapse or binary merging. This is exactly the time when we expect to get the strongest emission in gravitational waves. Since the ground based detectors are reaching sensitivities which allow the detection of gravitational wave signals from oscillating or unstable neutron stars the critical point for the onset of instabilities, the growth times of the instabilities and the exact frequencies of the emitted waves are urgently needed.

In this work we study within the general relativistic framework the oscillations and instabilities of fast and differentially rotating neutron stars in the so called Cowling approximation i.e. assuming a fixed spacetime. This is the first study of its kind since earlier works were using certain approximations e.g Newtonian theory [17] or slow rotation [18, 19]. Results, from fully nonlinear calculations exist only for the axisymmetric oscillation [20, 21]. Finally, the f -mode and the secular stability limits have been investigated in [22].

Recently, it has been found that in stars that rotate with a high degree of differential rotation an $m = 2$ dynamical instability can appear even for considerably low rotation rates ($T/|W| \sim O(10^{-2})$) as suggested in [23, 24]. In addition, an $m = 1$ dynamical instability has been identified for high degrees of differential rotation and soft equations of state [25, 26]. More recently, the discovery of $m = 1$ and $m = 2$ dynamical instability even for stiff equations of state [27] has been reported. Studies based on linear analysis [28, 29] suggest that low $T/|W|$ instabilities might be triggered when the corotation points of the unstable modes fall within the differentially rotating structure of the star.

The structure of the paper is as follows. In Section II we present the formulation that we have used to construct the equilibrium configurations. We then derive the perturbation equations in the general case of barotropic and

non-axisymmetric perturbations, which are numerically solved in Section III for the non-axisymmetric and barotropic case. Finally, in Section IV, we summarize the crucial results of this study.

Throughout the paper we use geometrical units $c = G = 1$.

II. FORMULATION OF THE PROBLEM

In this section we first show the basic principles of our problem. We then derive the evolution equations governing oscillations of perturbations on compact objects and the appropriate boundary conditions. Next, we present the equations of state we use for constructing equilibrium models and what kind of sequences we will consider. Finally, we explain how we solve the problem numerically.

A. Basic Principles

We study linear perturbations of rapidly and differentially rotating, relativistic neutron stars on a fixed background. First of all, this requires the computation of equilibrium configurations which are prescribed by their general-relativistic line-element and the specific form of the energy-momentum tensor. This last quantity describes the proper characteristics of the neutron star fluid and therefore, a certain equation of state has to be specified as well; we will address this issue later in this section.

The background metric of a fast rotating, relativistic star has to be stationary and axisymmetric and using spherical coordinates (r, θ, ϕ) , the line-element can be written as

$$ds^2 = -e^{2\nu} dt^2 + e^{2\psi} r^2 \sin^2 \theta (d\phi - \omega dt)^2 + e^{2\mu} (dr^2 + r^2 d\theta^2). \quad (1)$$

The four unknown functions ψ , μ , ν and ω are the metric potentials which depend on r and θ only and can be determined by solving the time-independent Einstein equations. Furthermore, for equilibrium models the radial and the polar component of the fluid's four-velocity u^μ vanishes while the remaining two components are related by the angular velocity Ω via

$$(u^t, u^r, u^\theta, u^\phi) = (u^t, 0, 0, \Omega u^t). \quad (2)$$

In general, the angular velocity Ω is a function of r and θ and although the exact form of $\Omega(r, \theta)$ is arbitrary to some extent, we adopt the so-called relativistic j -constant rotation law

$$A^2 (\Omega_c - \Omega) = \frac{(\Omega - \omega) r^2 \sin^2 \theta e^{2(\psi - \nu)}}{1 - (\Omega - \omega)^2 r^2 \sin^2 \theta e^{2(\psi - \nu)}}, \quad (3)$$

which satisfies the Rayleigh criterion for local dynamical stability against axisymmetric perturbations and which is commonly used in similar studies. [20, 30, 31]. Here, Ω_c is the angular velocity on the rotation axis and the free parameter A controls the degree of differential rotation. This quantity has units of length in the SI-system and specifies the length scale over which the angular velocity varies inside the star. As one can see from equation (3), the star is rotating uniformly again when A tends to infinity.

This definition of A is not convenient when considering sequences of equilibrium models with increasing rotation rate, since the radius of the star can vary by a factor of two which would be reflected in different degrees of differential rotation for each model. This issue can be circumvented by using a slightly modified parameter

$$\hat{A} := A/r_e, \quad (4)$$

which normalizes A by the equatorial radius r_e of the star; see also [20]. This definition maintains the same degree of differential rotation for all models along a sequence.

We furthermore assume the neutron star to be a perfect fluid without viscosity. In this case, the energy-momentum tensor has the form

$$T^{\mu\nu} = (\epsilon + p)u^\mu u^\nu + pg^{\mu\nu}, \quad (5)$$

where ϵ is the energy density, p is the pressure and $g^{\mu\nu}$ is the inverse metric. Energy and pressure are not independent quantities but they are related by an equation of state. In this study, we will focus on polytropic equations of state in the form of

$$\begin{aligned} p &= K\rho^\Gamma, \\ \epsilon &= \rho + Np. \end{aligned} \quad (6)$$

Here, ρ is the rest-mass density, K is the polytropic constant, N is the polytropic index and $\Gamma = 1 + 1/N$. For barotropic oscillations, pressure- and density-perturbations are connected by the speed of sound; $\delta p = c_s^2 \delta \epsilon$. In the case of polytropic equations of state, its value can be computed analytically and it is

$$c_s^2 = \frac{\Gamma p}{\epsilon + p}. \quad (7)$$

The thorough study of neutron star oscillations is very demanding and requires to solve the full, non-linear equations of general relativity. At this point, we will introduce some approximations in order to deal with a smaller set of equations and unknowns. First of all, we restrict the study to small perturbations around the equilibrium which allows us to linearize the equations. Second, we will use the so-called relativistic Cowling approximation, in which all metric perturbations are neglected. This effectively discards the space-time degrees of freedom and one only has to deal with the equations governing the motion of the fluid, which follow from the linear variation of the local law of energy-momentum-conservation

$$\delta(\nabla_\nu T^{\mu\nu}) = 0. \quad (8)$$

Since in the Cowling approximation, the covariant derivative is not affected by the fluid perturbation, equation (8) can be written as

$$\partial_\nu \delta T^{\mu\nu} + \Gamma_{\gamma\nu}^\mu \delta T^{\gamma\nu} + \Gamma_{\gamma\nu}^\nu \delta T^{\mu\gamma} = 0, \quad (9)$$

where $\delta T^{\mu\nu}$ is the perturbed energy-momentum tensor.

B. Perturbations Equations

The perturbation equations can be derived from equation (9) and for this, we will follow a very convenient formulation developed in [32, 33]. Instead of using the canonical fluid perturbation variables like velocity- or pressure-perturbation, the independent components of the perturbed energy-momentum tensor are utilized for the time-evolution.

To be more specific, we are directly evolving the variables $Q_1 := \delta T^{tt}$, $Q_2 := \delta T^{t\phi}$, $Q_3 := \delta T^{tr}$ and $Q_4 := \delta T^{t\theta}$ in time, using equation (9) to obtain the corresponding evolution equations. Additionally, we make use of an auxiliary variable $Q_6 := \delta T^{rr}$ which turns out to be a linear combination of Q_1 and Q_6 and which helps us in writing the resulting set of differential equations in a more compact way.

The final set of evolution equations is then given by

$$\begin{aligned} \partial_t Q_1 = & -\partial_\phi Q_2 - \partial_r Q_3 - \partial_\theta Q_4 \\ & - \left[e^{-2\nu+2\psi} r^2 \sin^2 \theta (\Omega - \omega) \partial_r \omega + \partial_r \psi + 2\partial_r \mu + 3\partial_r \nu + \frac{2}{r} \right] Q_3 \\ & - \left[e^{-2\nu+2\psi} r^2 \sin^2 \theta (\Omega - \omega) \partial_\theta \omega + \partial_\theta \psi + 2\partial_\theta \mu + 3\partial_\theta \nu + \frac{\cos \theta}{\sin \theta} \right] Q_4 \end{aligned} \quad (10a)$$

$$\begin{aligned} \partial_t Q_2 = & \Omega^2 \partial_\phi Q_1 - 2\Omega \partial_\phi Q_2 - \Omega \partial_r Q_3 - \Omega \partial_\theta Q_4 + \left[e^{-2\nu+2\mu} (\Omega - \omega)^2 - \frac{e^{-2\psi+2\mu}}{r^2 \sin^2 \theta} \right] \partial_\phi Q_6 \\ & - \left[e^{-2\nu+2\psi} r^2 \sin^2 \theta (\Omega - \omega) \omega \partial_r \omega + \partial_r (\Omega - \omega) + (3\Omega - 2\omega) \partial_r \psi \right. \\ & \quad \left. + 2\Omega \partial_r \mu + (\Omega + 2\omega) \partial_r \nu + (2\Omega - \omega) \frac{2}{r} \right] Q_3 \\ & - \left[e^{-2\nu+2\psi} r^2 \sin^2 \theta (\Omega - \omega) \omega \partial_\theta \omega + \partial_\theta (\Omega - \omega) + (3\Omega - 2\omega) \partial_\theta \psi \right. \\ & \quad \left. + 2\Omega \partial_\theta \mu + (\Omega + 2\omega) \partial_\theta \nu + (3\Omega - 2\omega) \frac{\cos \theta}{\sin \theta} \right] Q_4 \end{aligned} \quad (10b)$$

$$\begin{aligned}
\partial_t Q_3 &= -\Omega \partial_\phi Q_3 - \partial_r Q_6 \\
&\quad - \left[e^{-2\mu+2\nu} \partial_r \nu + e^{-2\mu+2\psi} r \sin^2 \theta \left[(\Omega^2 - \omega^2) (1 + r \partial_r \psi) - r \omega \partial_r \omega \right] \right] Q_1 \\
&\quad - \left[e^{-2\mu+2\psi} r \sin^2 \theta \left[r \partial_r \omega - 2(\Omega - \omega)(1 + r \partial_r \psi) \right] \right] Q_2 \\
&\quad - \left[\partial_r \nu + 2 \partial_r \mu + e^{-2\nu+2\psi} r \sin^2 \theta (\Omega - \omega)^2 (1 + r \partial_r \psi) \right] Q_6
\end{aligned} \tag{10c}$$

$$\begin{aligned}
\partial_t Q_4 &= -\Omega \partial_\phi Q_4 - \frac{1}{r^2} \partial_\theta Q_6 \\
&\quad - \frac{1}{r^2} \left[e^{-2\mu+2\nu} \partial_\theta \nu + e^{-2\mu+2\psi} r^2 \sin \theta \left[(\Omega^2 - \omega^2) (\cos \theta + \sin \theta \partial_\theta \psi) - \sin \theta \omega \partial_\theta \omega \right] \right] Q_1 \\
&\quad - \frac{1}{r^2} \left[e^{-2\mu+2\psi} r^2 \sin \theta \left[\sin \theta \partial_\theta \omega - 2(\Omega - \omega) (\cos \theta + \sin \theta \partial_\theta \psi) \right] \right] Q_2 \\
&\quad - \frac{1}{r^2} \left[\partial_\theta \nu + 2 \partial_\theta \mu + e^{-2\nu+2\psi} r^2 \sin \theta (\Omega - \omega)^2 (\cos \theta + \sin \theta \partial_\theta \psi) \right] Q_6
\end{aligned} \tag{10d}$$

Additionally, the value of Q_6 in terms of Q_1 and Q_2 is calculated by

$$\begin{aligned}
Q_6 &= \frac{e^{-2\mu+2\nu} c_s^2}{1 - e^{-2\nu+2\psi} r^2 \sin^2 \theta (\Omega - \omega)^2 c_s^2} \\
&\quad \times \left[\left[1 + e^{-2\nu+2\psi} r^2 \sin^2 \theta (\Omega^2 - \omega^2) \right] Q_1 - 2e^{-2\nu+2\psi} r^2 \sin^2 \theta (\Omega - \omega) Q_2 \right].
\end{aligned} \tag{11}$$

Since equilibrium stars are axisymmetric, but not necessarily spherically symmetric in case of rapid rotation, we will not use an angular decomposition into spherical harmonics but instead only separate the azimuthal part according to

$$Q_i(t, r, \theta, \phi) := \tilde{Q}_i(t, r, \theta) e^{im\phi} \quad \text{for } i = 1, \dots, 4.$$

Due to this decomposition, the evolution equations (10a)-(10d) are only slightly modified and we just have to perform the substitution $\partial_\phi \rightarrow im$. In the following discussion, we will omit the tilde to avoid confusion.

C. Boundary Conditions

In order to close the system of equations (10a)-(10d), one needs to impose proper boundary conditions. In the study presented here, this boundary consists of the stellar surface, the equatorial plane and the rotation axis. Special care has to be taken of the origin which is mapped onto a boundary line in spherical coordinates.

Let us first consider the stellar surface, where the radial and polar perturbation variables Q_3 and Q_4 are zero by virtue of their definition

$$\begin{aligned}
Q_3 &= \delta T^{tr} = (\epsilon + p) u^t \delta u^r = 0 \\
Q_4 &= \delta T^{t\theta} = (\epsilon + p) u^t \delta u^\theta = 0,
\end{aligned}$$

because pressure and energy density vanish there. Q_1 and Q_2 however have to remain continuously differentiable there.

On an axisymmetric background, each oscillation mode can be assigned to one of two possible parity classes which behave differently under space inversion; see [34]. Due to the decomposition with respect to the azimuthal angle ϕ , the behaviour under reflection with respect to the equatorial plane is also well-defined and the two parity classes obey different conditions in the equatorial plane. For one class of modes, the perturbation variables Q_1 , Q_2 and Q_3 are all even, whereas Q_4 is odd. The $l = m$ fundamental mode belongs to this class, since the angular part of the pressure perturbation behaves like the scalar spherical harmonic Y_l^m , which is even as well. In contrast, the perturbation variables of modes belonging to the second class behave exactly the other way around. The $l = m$ r-mode is an example for a mode of this specific class. We therefore apply different boundary conditions along the equatorial plane, depending on which class of modes we want to excite.

For deriving the boundary conditions along the rotation axis and at the origin, we use a representation of pressure and velocity perturbations according to [35]. These expressions were derived in the so-called slow-rotation approximation where one neglects high order effects of rotation, but the relevant coupling between the two different mode

classes is already included within this approach and does not change at all in rapidly rotating stars. The boundary conditions we use in this study for discussing spherically symmetric (mostly for code verification purposes) and quadrupolar perturbations are shown in Tables I and II.

$ m $	$Q_1 _{r=0}$	$Q_2 _{r=0}$	$Q_3 _{r=0}$	$Q_4 _{r=0}$
0	finite	finite	0	0
2	0	0	0	0

TABLE I: Boundary conditions for the perturbation variables at the origin.

$ m $	$Q_1 _{\theta=0}$	$Q_2 _{\theta=0}$	$Q_3 _{\theta=0}$	$Q_4 _{\theta=0}$
0	finite	finite	finite	0
2	$\partial_\theta = 0$	$\partial_\theta = 0$	0	0

TABLE II: Boundary conditions for the perturbation variables along the rotation axis.

D. Equilibrium Models

For constructing the equilibrium models, we use the `rns`-code developed by Stergioulas [36, 37], which was later extended to handle differential rotation. Furthermore, we are using three different equations of state which were already used for the study of uniformly rotating stars in [38, 39] and for which we construct equilibrium sequences with a constant central rest-mass density. All three EoS are polytropic ones; but two of them are fits to tabulated equations of state and together they cover very well the expected range of neutron star masses and radii, see for example [40, 41].

For all equations of state, we consider uniformly rotating models as well as their differentially rotating counterparts for different values of \hat{A} . All sequences start with a non-rotating model for which the axis ratio r_p/r_e of polar to equatorial coordinate radius equals 1. Subsequent models are computed by decreasing this ratio by a factor of 0.05 until the Kepler limit is reached.

The EoS B is a widely used polytropic equation of state with parameters $\Gamma = 2$ and $K = 100$ in units of $G = c = M_\odot = 1$, and here we consider the commonly used BU sequence, for which the dimensionless central rest-mass density is given by $\rho_c = 1.28 \times 10^{-3}$. This leads to standard values for the mass and the radius of the non-rotating model; a detailed list with properties of the BU models and their differentially rotating counterparts with $\hat{A} = 1$ (B sequence) is given in [20]. The non-rotating model, which is labelled BU0, has a gravitational mass of $M = 1.4 M_\odot$ and a circumferential radius of $R_e = 14.16$ km. The fastest rotating member of the uniformly rotating B sequence has an axis ratio of $r_p/r_e = 0.58$, a slightly increased mass of $M = 1.695 M_\odot$ and an equatorial radius of $R = 19.96$ km.

When the star is differentially rotating (the following discussion refers to the B sequence with $\hat{A} = 1$), these changes become even more evident. Due to the fact that differential rotation allows to store a large amount of angular momentum near the rotation axis, the value of $T/|W|$ can reach much higher values.

Furthermore, the star can become more compact near the rotation axis in comparison to the corresponding uniformly rotating star which results in a very high mass. The axis ratio for the most rapidly rotating model B12 can be decreased down to a value of 0.4 with a mass of $M = 2.532 M_\odot$ which is an increase of 50 % when compared to the uniformly rotating model BU9.

As already mentioned, we additionally study two other equations of state which are polytropic fits to the tabulated EoS A and EoS II, see [42–44] for more details. The oscillation frequencies of neutron star models governed by these EoS have already been investigated in [38]. The fitting parameters for EoS II are $\Gamma = 2.34$ and $K = 1186$ and $\Gamma = 2.46$ and $K = 1528$ for EoS A again in units where $G = c = M_\odot = 1$. For both EoS, we choose models which are very close to their maximum mass; e. g. see Figure 9 in [38]. Apparently, the models for EoS A and EoS II have smaller radii and larger masses compared to the B sequences. A detailed list of the differentially rotating background models is shown in Table III.

E. Numerical Implementation

After decomposing the perturbed quantities with respect to ϕ , the resulting evolution equations form a two-dimensional problem in the spherical coordinates r and θ . As radial grid coordinate we choose a mapping of the

Model	r_p/r_e	Ω_c (kHz)	Ω_e (kHz)	R_e (km)	M (M_\odot)	$T/ W $
B0	1.00	0.000	0.000	14.16	1.400	0.000
B1	0.95	3.657	1.352	14.40	1.437	0.013
B2	0.90	5.226	1.917	14.65	1.478	0.026
B3	0.85	6.473	2.354	14.93	1.525	0.040
B4	0.80	7.568	2.724	15.23	1.578	0.055
B5	0.75	8.581	3.053	15.55	1.640	0.070
B6	0.70	9.555	3.352	15.90	1.713	0.087
B7	0.65	10.526	3.632	16.26	1.798	0.105
B8	0.60	11.537	3.899	16.63	1.899	0.124
B9	0.55	12.651	4.166	16.99	2.020	0.144
B10	0.50	13.984	4.449	17.29	2.167	0.165
B11	0.45	15.772	4.785	17.42	2.341	0.186
B12	0.40	18.508	5.245	17.20	2.532	0.207
II0	1.00	0.000	0.000	11.71	1.908	0.000
II1	0.95	6.865	1.960	11.82	1.943	0.013
II2	0.90	9.935	2.796	11.93	1.982	0.026
II3	0.85	12.481	3.454	12.04	2.025	0.041
II4	0.80	14.830	4.026	12.15	2.072	0.056
II5	0.75	17.131	4.549	12.25	2.124	0.071
II6	0.70	19.490	5.043	12.34	2.181	0.087
II7	0.65	22.011	5.525	12.41	2.241	0.104
A0	1.00	0.000	0.000	9.53	1.614	0.000
A1	0.95	8.751	2.431	9.61	1.644	0.013
A2	0.90	12.681	3.468	9.70	1.676	0.027
A3	0.85	15.954	4.285	9.78	1.712	0.041
A4	0.80	18.989	4.997	9.87	1.751	0.056
A5	0.75	21.977	5.647	9.94	1.794	0.071
A6	0.70	25.056	6.264	10.00	1.840	0.087
A7	0.65	28.360	6.865	10.04	1.888	0.103

TABLE III: Stellar properties of the differentially rotating models with $\hat{A} = 1$. Ω_c and Ω_e are the angular velocities along the rotation axis and at the equator respectively, R_e is the equatorial circumferential radius and M the gravitational mass.

form $s = 0.5 (r/r_e)^2$, which allows for stable time evolutions with much less artificial viscosity when compared to the original radial grid coordinate of the `rns`-code. For the angular grid coordinate we choose between $t = \cos(\theta)$ and $t = 1 - 2\theta/\pi$ depending on the degree of differential rotation. In the Cowling approximation, only the interior of the star needs to be considered and this means that $s \leq 0.5$ for all t . In the non-rotating limit, the surface of the star coincides exactly with the gridline at $s = 0.5$.

However, this choice of grid parameters poses a small challenge when applying boundary conditions on the surface of a rapidly rotating star, since in this case the surface lies in between the grid points of our computational domain. One therefore has to approximate the outer boundary in a proper way which is done here in the following manner: For each angular direction, we monitor the variation of the energy density when moving radially outwards and set the surface at this particular angle to be the first grid point where the energy density vanishes. The boundary conditions are then applied to these set of grid points. Depending on the shape of the star, one may have to increase the angular resolution of the grid in order to get an accurate approximation of the stellar surface. As already mentioned before, we use two different angular grid coordinates. While the mapping $t = \cos(\theta)$ is appropriate for small degrees of differential rotation, for higher degrees $t = 1 - 2\theta/\pi$ is the better choice.

Concerning the time-evolution scheme, we use standard central differences for spatial discretization and the classical fourth-order Runge-Kutta method as time integrator. Similar to previous studies within the same perturbative framework [38, 39], this code is prone to numerical instabilities around the origin of the star, which can be cured by using standard second-order Kreiss-Oliger dissipation [45]. Depending on the resolution of the grid, we always use the smallest amount of artificial viscosity in order to keep the effect of this purely numerical additive as marginal as possible. Typically, the simulations were performed using a grid size of 120×90 points; in this case, the dissipation coefficients are of the order of 10^{-4} . As it turned out, the mode frequencies do not change significantly when increasing

either the resolution of the computational domain or the amount of artificial viscosity. Additionally, the utilization of the Runge-Kutta method as time-integrator allowed for a further decrease in the amount of dissipation when compared to the Iterated Crank-Nicholson scheme used in previous studies. This also leads to a considerably slower numerical damping of the oscillations.

The code is numerically stable for simulations up to some hundreds of milliseconds. Usually, our simulations cover roughly 100 ms, resulting in a frequency resolution of $\Delta f \approx 10$ Hz. We then extract the eigenfrequencies from the time evolution by performing a Fast Fourier Transform on the obtained time series at some arbitrary points inside the star. For an unambiguous identification of a specific mode, we use Fourier transforms at each single point inside the star in order to construct the entire two-dimensional eigenfunction. Once we determined an eigenfrequency by means of the Fourier spectrum at a certain point, we track the amplitude of the Fourier transform for all grid points at this particular frequency which gives us the modulus of the corresponding eigenfunction. A sign flip in the eigenfunction is reflected by a shift of π in the Fourier transform's argument. With the eigenfunctions extracted, we are also able to perform mode recycling [21, 38] in order to enhance a particular mode in the oscillation pattern, typically resulting in a more accurate frequency determination.

III. RESULTS

We now present the results obtained with our method as outlined in the previous sections. First, we will test it on uniformly rotating models to check the accuracy of the newly developed code. We then turn to differentially rotating stars and investigate the effects for both small and large degrees of differential rotation on the onset of the CFS unstable fundamental quadrupolar mode. Finally, we will take a look at the generically unstable r-mode in differentially rotating stars.

A. Uniform Rotation

We first want to consider perturbations of uniformly rotating stars mostly for code verification purposes. Barotropic oscillations of this type have already been studied extensively in [38] with the very same polytropic equations of state considered in this study. However, here we use a completely different set of perturbation equations, different coordinate systems and numerical methods. Still, both axisymmetric and non-axisymmetric mode frequencies can be reproduced with a very good accuracy; the discrepancy between the two different codes is below 2% in all cases.

As an example, Figure 1 shows a comparison between results obtained in the present study and published values for the fundamental quadrupolar f-mode splitting found in [38]. The sequences of background models in these two studies are identical, so a good means in order to estimate the differences between the two methods is to observe the off-centering of the triangles, which are the data points from the current study, from its enclosing circles, which represent the literature values.

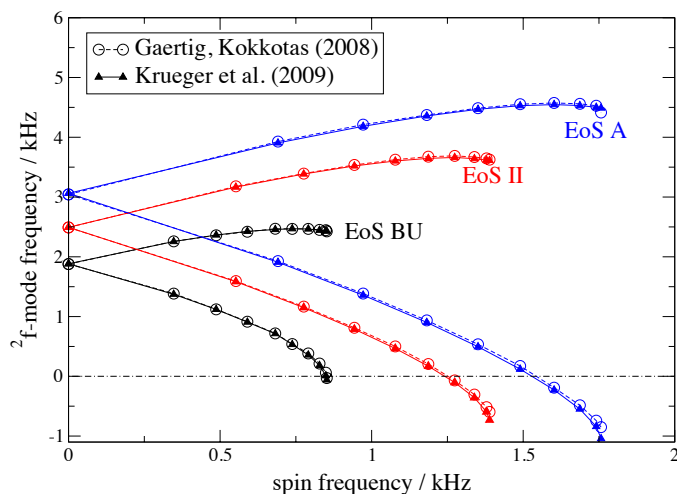


FIG. 1: Comparison of the fundamental mode splitting for $l = |m| = 2$ and different EoS. Differences can be monitored by the shift of the triangles (present study) with respect to its enclosing circles (results from [38]).

Obviously, only for very high rotation rates there are some deviations; otherwise the two codes provide nearly identical results.

We also checked the frequencies of the second class of oscillation modes which are present in a barotropic, perfect fluid star as soon as rotation sets in; these are the inertial modes. Again, the agreement between the two codes is excellent; a comparison with frequencies found in [46] also shows a good agreement (see [47] for more details).

B. Axisymmetric Modes of Differentially Rotating Stars

Next, we consider axisymmetric perturbations on differentially rotating backgrounds and compare the results with [20], who investigated the same problem with a non-linear code applied to small perturbations.

Figure 2 shows the effect of rotation on the three fundamental modes F, 2f and 4f as well as the first overtones H_1 and 2p_1 for both uniformly and differentially rotating models of the BU and B sequences. As already discussed in Section IID, differential rotation allows for a higher mass of equilibrium models compared to their uniformly rotating counterparts and the corresponding value of $T/|W|$ can reach significantly higher values. This is the reason why the dashed curves for uniformly rotating stars terminate already at a rather low $T/|W|$ in Figure 2, which is similar to Figure 5 in [20].

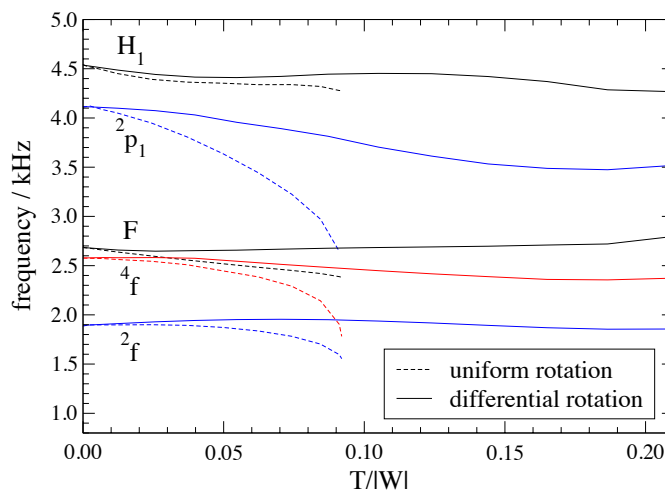


FIG. 2: Mode frequencies of several quasi-radial ($m = 0$) modes for uniformly and differentially rotating stars of the B sequence.

As one can clearly see, the mode frequencies of differentially rotating models are typically larger than the corresponding frequencies for the uniformly rotating sequence. The reason for this is that differentially rotating stars usually have a smaller equatorial radius than their uniformly rotating counterparts with the same $T/|W|$. Therefore, the crossing time of acoustic waves, like the f - and higher order p -modes, is lowered which leads to a higher oscillation frequency.

The agreement with the data provided in [20] is very good; the relative difference is below 2.5% for all frequencies. However, we disagree about the interpretation of the so-called F_{II} -mode which was found in [20] and was interpreted as a possible splitting of the fundamental quasi-radial mode in differentially rotating stars; a reason for this might be the Cowling approximation which violates energy and momentum constraints.

When we reiterated this simulation with the code presented in this study, we also found peaks in the Fourier spectrum at the very same frequencies published in [20] for the F_{II} -mode. However, after extracting the corresponding eigenfunction, we are convinced that this F_{II} -mode is nothing more than the 4f -mode. The frequencies of both the F -mode and the 4f -mode are nearly indistinguishable in slowly rotating stars; the difference is around 100 Hz which makes a reliable assignment of the eigenfunctions a difficult task. Fortunately, it turned out that the eigenfunction of δu^θ is a very good means to discriminate between the two quasi-radial modes.

Figure 3 shows contour lines of the time-evolution variable $Q_4 \sim \delta u^\theta$ (see section IIC) projected on the (s, t) -plane for the F - and the 4f -mode. In both panels, these modes are compared for a very slowly rotating model (solid line) with an axis ratio of $r_p/r_e = 0.999$ and a B3 neutron star (dashed line). The step-like curve on the right side of both panels is the approximated surface of the B3 model. As already discussed in Section IIE, only for non-rotating stars the stellar surface coincides with $s = 0.5$. Within the grid-resolution used in Figure 3, this is still true for the slowly rotating model considered here. The rotation rate of the B3 model is also the reason, why the contours of Q_4 are

shifted to smaller radial distances in this case. Apart from that, the shapes of the eigenfunctions are identical in both panels.

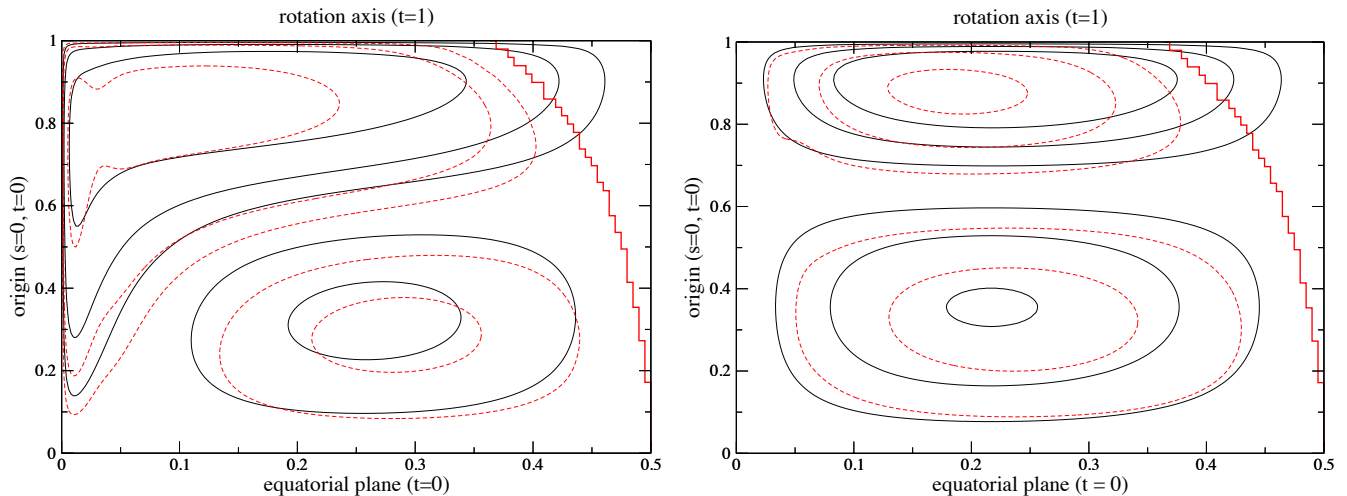


FIG. 3: *Left Panel:* Contours of the Q_4 -eigenfunction of the F-mode for a slowly rotating B model with $r_p/r_e = 0.999$ (solid) and a B3 neutron star (dashed). The step-like curve on the right approximates the stellar surface for the B3 model. *Right Panel:* Same for the 4f -mode.

Actually, this issue about erroneous mode identification will always be present for various stellar models and certain modes. In the case shown here, the problem can be resolved if one drops the Cowling-approximation because this approximation overestimates the frequencies of the F-modes, making them nearly identical to those of the 4f -mode for this particular sequence of equilibrium models. However, the problem will still be there for different modes or stellar models and thus the analysis presented here is the only meaningful way to distinguish between certain modes.

C. Non-Axisymmetric f-modes in Differentially Rotating Stars

We next turn to non-axisymmetric perturbations on differentially rotating stars. In the following discussion, we will mostly focus on the quadrupolar fundamental mode in particular, because this is the lowest order mode which is able to emit gravitational waves. For uniformly rotating stars, the 2f -mode is also prone to the secular CFS instability, but typically only for models which rotate close to their mass-shedding limit. The neutral point for the onset of the instability is considerably lower for modes with higher azimuthal index m . However, it turns out that the growth time of these modes is considerably larger than the viscous timescales. Therefore, one usually studies the 2f -mode exclusively.

In Table IV we show the eigenfrequencies of the 2f -mode for the sequence B and a degree of differential rotation of $\hat{A} = 1.0$. As one can see, the star becomes unstable at a point between the B8 and the B9 model. The values in Table IV have been compared with preliminary results from non-linear evolution codes and show a good agreement [48].

One may now ask, how this behaviour changes for different degrees of differential rotation. As we know, the uniformly rotating model, which corresponds to $\hat{A}^{-1} = 0.0$, becomes secularly unstable just around its mass-shedding limit while for $\hat{A}^{-1} = 1.0$ this happens at roughly 65% of the highest possible $T/|W|$ for a stable equilibrium.

Figure 4 shows the splitting of 2f -mode for four different degrees of differential rotation, starting from the uniform rotation limit with $\hat{A}^{-1} = 0.0$ to a value of $\hat{A}^{-1} = 1.43$. First of all, one can see that differential rotation leads to an increase in the mode frequencies compared to the uniformly rotating case; something we already observed for axisymmetric modes, see Figure 2. Second, a high degree of differential rotation favours the onset of the CFS instability in the sense that the neutral point is reached at a smaller fraction of the maximum allowed $T/|W|$.

Third, for sufficiently large values of \hat{A}^{-1} , the mode frequencies of the corotating branch always increase as can be seen from Figure 4 for $\hat{A}^{-1} \gtrsim 1.0$. This is in strong contrast to the uniformly rotating case where the frequencies of the prograde travelling modes reach a local maximum before they decrease again; see also Figure 2. If the background models allowed for high rotation rates, the frequency of the corotating branch would decrease even more and at some value of $T/|W|$ merge with the frequency of the retrograde travelling mode which is dragged forward by rotation in the inertial frame. This point then signals the onset of the dynamical bar-mode instability.

model	2f (kHz)	
	$m = 2$	$m = -2$
B0	1.884	1.884
B1	1.428	2.239
B2	1.204	2.363
B3	1.015	2.449
B4	0.841	2.515
B5	0.673	2.567
B6	0.505	2.611
B7	0.338	2.648
B8	0.162	2.683
B9	-0.026	2.726
B10	-0.246	2.788

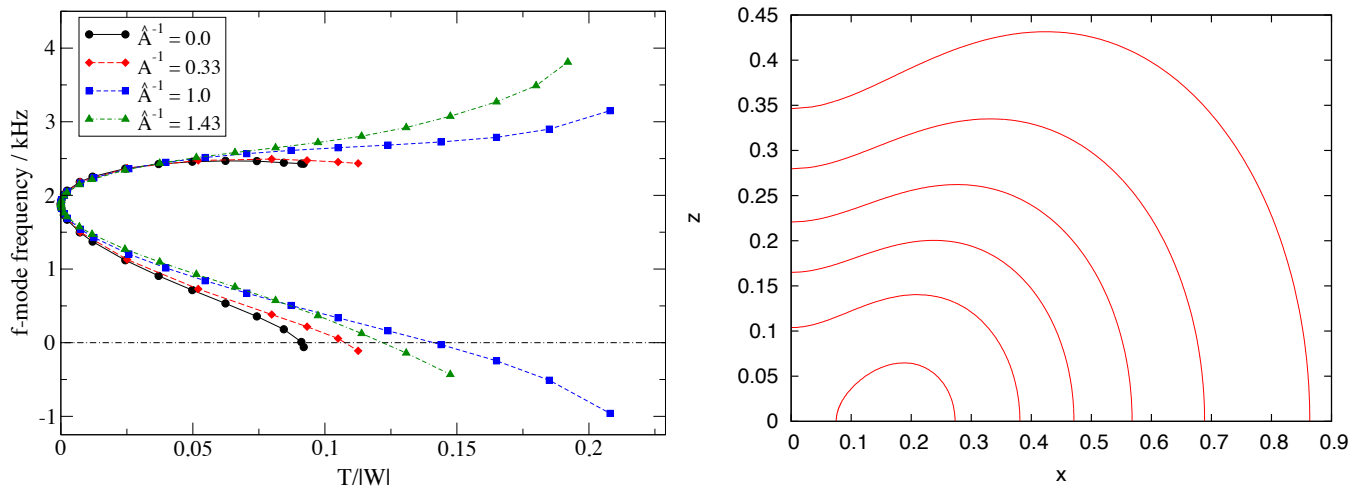
TABLE IV: Frequencies of the 2f -mode for the B sequence and $\hat{A} = 1.0$.

FIG. 4: *Left Panel:* Splitting of the 2f -mode for different degrees of differential rotation \hat{A} . All equilibrium sequences are based on EoS B. *Right Panel:* Density contour lines of the most rapidly rotating model B12. The outermost line corresponds to the surface of the star, the z-axis represents the rotation axis.

The situation changes in the case of differential rotation. Depending on the degree of differential rotation and the rotation rate, there is a transition of the axisymmetric equilibrium configuration from an oblate spheroid with its maximum energy-density and pressure at the center of the star towards a toroidal configuration where these peak values are reached along a ring-like structure in the equatorial plane; see the right panel of Figure 4 for a density-contour plot of the most rapidly rotating model with $\hat{A}^{-1} = 1.0$. This change in the topology of the background model leads to an increase in the frequencies of the corotating branch which of course sets in earlier for equilibrium configurations with large degrees of differential rotation since in this case, the toroidal structure of the background star is already realized for comparatively small values of $T/|W|$. One should also note that while the sequences considered here are still configurations with the same central energy density, the maximum value of the energy density is reached outside the center of the star as soon as the transition to a toroidal structure sets in.

1. Small Degree of Differential Rotation

We want to discuss the onset of the CFS-instability a bit more in the regime of weakly differential rotation, i. e. small values of \hat{A}^{-1} . As one can see clearly from Figure 4, the critical value of $\beta := T/|W|$, where the neutral point of the secular instability is reached, typically increases with the degree of differential rotation. In order to estimate whether differential rotation favours the onset of the CFS mechanism, one also needs to know the maximum value β can attain. In differentially rotating stars, a large amount of angular momentum can be stored in inner layers close to the rotational axis. This also means, that the highest possible value of β increases as well.

In the subsequent discussion, we will restrict our simulations to smaller values of \hat{A}^{-1} for the following reason: Since we later want to normalize the critical value for the onset of the CFS instability β_c with the corresponding value β_s at the mass-shedding limit, we need dynamically stable equilibrium models at this Kepler frequency; otherwise the normalization would not make much sense. It turns out, that our particular choice of background models is dynamically unstable to radial oscillations for comparatively small values of \hat{A}^{-1} . For example, the B sequence is dynamically unstable before reaching the mass-shedding limit for $\hat{A}^{-1} \gtrsim 0.7$. It is worth pointing out, that the endpoint of the B model series in Table III, i. e. model B12, does not terminate because of the mass-shedding limit but because of dynamical instabilities. The same is also true for sequences A and II; due to the higher initial masses, this effect is even more pronounced there.

Figure 5 shows, how β_c and β_s change with the degree of differential rotation. As already conjectured, both values increase with \hat{A}^{-1} and the slope of β_s is even larger than the one for β_c . This confirms our initial assumption, that the onset of the secular CFS instability is eased for larger degrees of differential rotation.

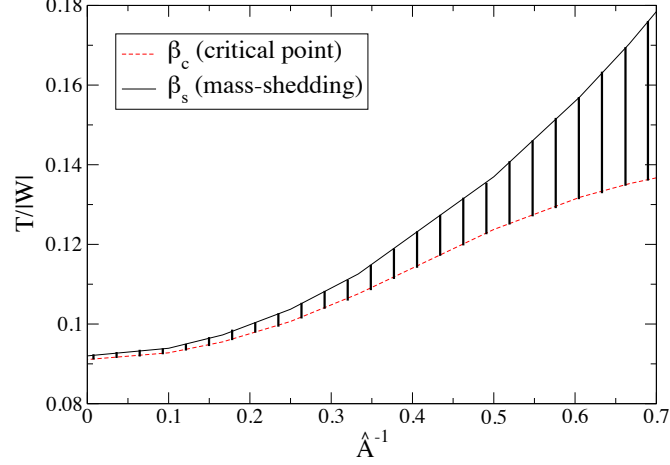


FIG. 5: The values of β_c and β_s as a function of \hat{A}^{-1} for the 2f -mode and the B model series. The filled area marks the CFS-unstable region.

In Figure 6, we plot the value of $\tilde{\beta}_c := \beta_c/\beta_s$ for three different modes of the B sequence as function of the degree of differential rotation \hat{A}^{-1} . This normalization of the critical $T/|W|$ is similar to the common procedure for uniformly rotating stars, where one typically measures the angular velocity of the star in units of the Kepler-frequency.

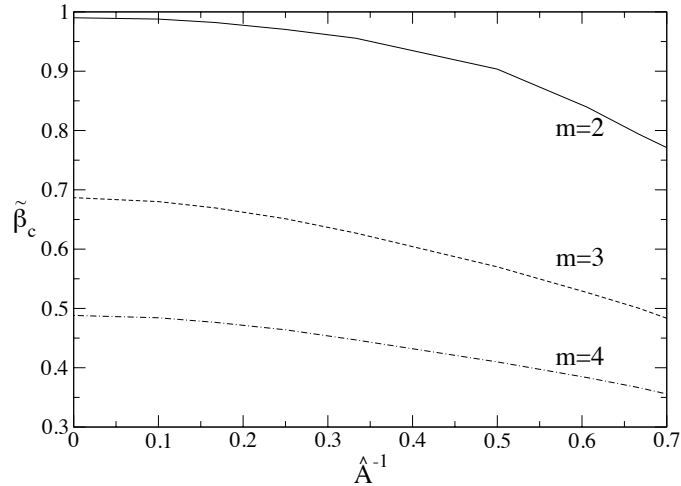


FIG. 6: The normalized, critical value $\tilde{\beta}_c$ for the onset of the CFS instability of the B sequences as a function of the degree of differential rotation \hat{A}^{-1} for $m = 2, 3, 4$.

Keep in mind that the uniformly rotating limit is reached for $\hat{A}^{-1} = 0.0$. As we already have seen in Figure 4, in this case the 2f -mode becomes unstable just around its mass-shedding limit which corresponds to $\tilde{\beta}_c \approx 1.0$. It has

already been mentioned in Section III C that higher order modes become secularly unstable even earlier and this is also reflected in Figure 6. For example, in the limit of uniform rotation, the 3f -mode gets unstable at roughly 70% of the critical $T/|W|$, the 4f -mode even at approximately 50%. However, it has already been noted that the growth time for the instability will increase for modes with larger m and is most likely suppressed by viscosity.

When we trace the value of $\tilde{\beta}_c$ for the various fundamental modes and several degrees of differential rotation, we see clearly that for larger values of \hat{A}^{-1} , the critical $T/|W|$ decreases invariably for all modes; i. e. the onset of the instability is favoured in these cases.

We also studied the behaviour of $\tilde{\beta}_c$ for the stiffer equations of state EoS A and EoS II. The actual equilibrium models we considered are very close to their maximum allowed mass and therefore we can increase the differential rotation parameter \hat{A} only to a very moderate degree of around $\hat{A} \approx 2.3$ because models with a higher degree of differential rotation will be dynamically unstable. Figure 7 again shows a plot of $\tilde{\beta}_c$ for different values of \hat{A}^{-1} , but this time for the fundamental quadrupolar mode and the three different polytropic equations of state that were considered in this study. As already found in [38] and one can also see in Figure 1, the CFS instability acts much earlier in the more compact sequences A and II.

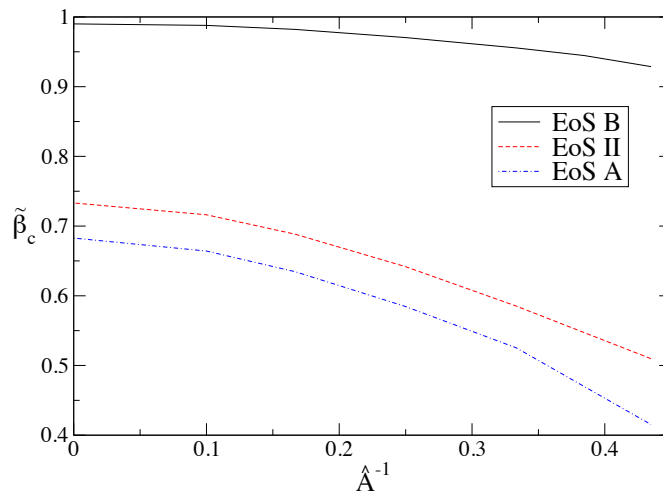


FIG. 7: The normalized, critical value $\tilde{\beta}_c$ for the onset of the CFS instability of the 2f -mode for different equations of state.

It is worth noticing that the influence of differential rotation is even more pronounced for these sequences when compared to sequence B. As one can see from Figure 7, the critical curves for EoS A and EoS II decrease more strongly than the corresponding curve for the less compact EoS B series. As an example, while increasing the differential rotation parameter from $\hat{A}^{-1} = 0.0$ to $\hat{A}^{-1} = 0.43$, the value of $\tilde{\beta}_c$ is lowered only by 6% for sequence B but by 30% for sequence II and even 39% for sequence A. Therefore, the onset of the CFS instability is also eased by the compactness of the neutron star when differential rotation is considered.

2. Large Degree of Differential Rotation

As we discussed in the previous section, equilibrium sequences with a high degree of differential rotation ($\hat{A}^{-1} \gtrsim 1$) terminate due to dynamical instabilities with respect to radial oscillations; see [49] for a study on the maximum mass of differentially rotating neutron stars. Therefore, it does not make sense to define the mass-shedding value β_s , and correspondingly the same holds for the normalized quantity $\tilde{\beta}_c$. Nevertheless, the sequences still reach the neutral point β_c for the onset of the CFS instability of the fundamental quadrupolar mode.

In Figure 8, we show β_c of the quadrupolar f-mode for the three equations of state EoS B, EoS II and EoS A as well as for an additional one which we label EoS C and which has an intermediate polytropic exponent of $\Gamma = 2.18$ and $K = 400$ in the same units as for the other equations of state.

In contrast to the previous section, we continue to increase the degree of differential rotation up to $\hat{A}^{-1} = 1.75$. When moving from rigid rotation to a small degree of differential rotation, the value of β_c increases for each equation of state. Any sequence considered in this study reaches a local maximum which is located at $\hat{A}^{-1} = 0.89$ for the B-sequence and $\hat{A}^{-1} = 0.78$ for EoS C while EoS II and EoS A reach it considerably earlier at $\hat{A}^{-1} = 0.74$ and $\hat{A}^{-1} = 0.69$, respectively.

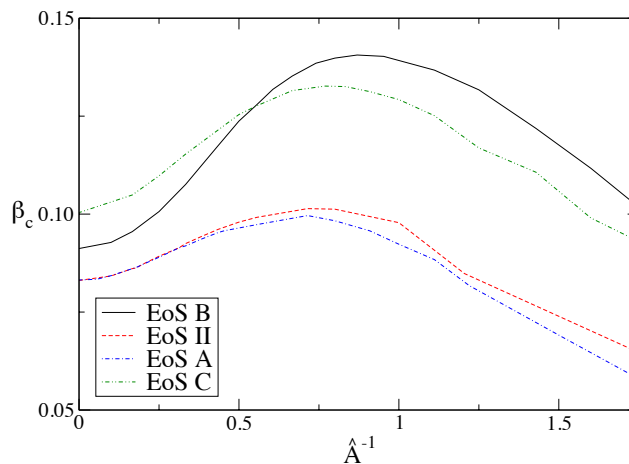


FIG. 8: The critical value β_c of the 2f -mode for four different equations of state.

For higher degrees of differential rotation, the value of $T/|W|$ for the neutral point decreases. Again, similar to the observations we made for small degrees of differential rotation, this effect is more pronounced for the more compact models of the stiffer equations of state EoS II and EoS A. As one also can see from Figure 8, the critical value for the C, A and II sequences even drop clearly below the value for rigid rotation. For EoS A and EoS II, this happens roughly at around $\hat{A}^{-1} \approx 1.2$ while $\hat{A}^{-1} \approx 1.5$ for EoS C. In contrast to this, while also decreasing in amplitude, the value of β_c for the B-sequence does not drop below the corresponding value of the uniform rotation limit, at least not up to $\hat{A}^{-1} = 1.75$ which is the endpoint of the sequences in Figure 8.

A similar investigation has already been carried out for Newtonian polytropes [17], and we qualitatively agree with their results. Further comparisons are not possible for various reasons; most crucial is the different definition of the parameter \hat{A} which controls the degree of differential rotation.

D. Rotational Modes in Differentially Rotating Stars

Another very important class of oscillation modes are the r-modes, because they are generically CFS unstable [50]. Here, we only consider the $l = m = 2$ r-mode. Since the r-mode is purely axial in the non-rotating limit, it belongs to that class of modes whose pressure variation has odd parity under reflection with respect to the equatorial plane.

In Figure 9 we show the frequencies of the r-mode along sequences using EoS B or for different degrees of differential rotation. We normalize them by the central angular velocity Ω_c of the corresponding star, as it has already been done in [51]. This kind of normalization is suggested by the relation $\sigma = 4/3 \Omega$ which is valid in Newtonian theory, where σ is the r-mode's angular frequency measured in the inertial frame and Ω the angular velocity of the star.

First, we inspect the solid curve representing the rigidly rotation case, i.e. $\hat{A}^{-1} = 0$. Concerning the value of σ/Ω_c in the non-rotating limit, which is approximately 1.43, we observe a clear deviation from Newtonian theory. However, this is consistent with general relativistic corrections to the Newtonian result. It can be shown [52] that in the non-rotating limit the Newtonian value of $4/3$ is increased by a term which is proportional to the frame-dragging potential ω .

The curves corresponding to the differentially rotating sequences have lower values, because the central angular velocity increases compared to the uniformly rotating ones, and this effect becomes even stronger the higher the degree of differential rotation is. On the other hand, the angular velocity at the equator, Ω_e , is lowered so that a normalization by this quantity would move the lines in the other direction. Finally, we chose to normalize by the central angular velocity in order to compare qualitatively with Newtonian findings [51]. We find that the qualitative behaviour is the same.

Moreover, we explicitly computed the eigenfunction of the δu^θ velocity perturbation. According to the Newtonian results in [51], we find that the amplitude of the eigenfunction gets confined towards the surface of the star as differential rotation is increased.

Earlier studies based on the slow rotation approximation also suggested that there might be a continuous spectrum for the r-modes [53–55]. More recently the same claim has been made in the study of differentially rotating relativistic stars in the slow-rotation approximation [19]. Here, in agreement with earlier results for uniformly rotating stars [38, 39], we have found no trace of the continuum spectrum. This result does not exclude its existence, because

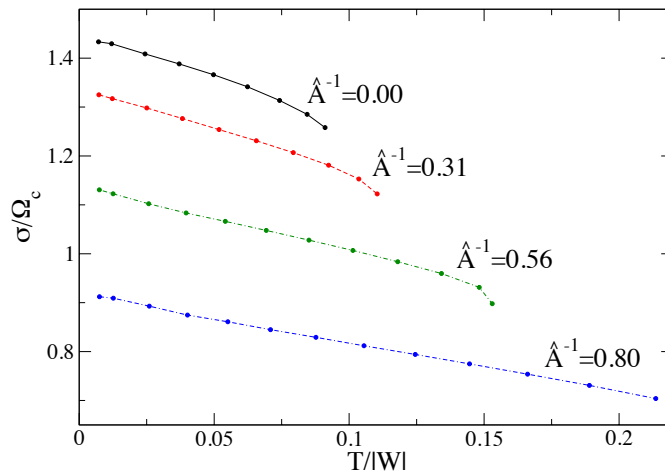


FIG. 9: Frequencies of the r-mode for several B sequences with different degrees of differential rotation. The frequencies are normalized by the central angular velocity Ω_c .

the continuum can co-exist with discrete modes. Especially here we excite the oscillation by using an approximate eigenfunction of the mode under study, then by repeated mode recycling we force the star to oscillate on this specific mode alone in order to extract both the eigenfrequency and the eigenfunction with highest possible accuracy. This way we exclude excitation of any other mode or continuum, still we should stress that no numerical calculation of fast rotating relativistic star modes to date both in linear and non-linear form has shown the presence of a continuous spectrum.

IV. SUMMARY

In this work we performed time evolutions of oscillations of differentially and rapidly rotating, relativistic stars using the Cowling approximation, and we were able to investigate both axisymmetric and non-axisymmetric perturbations. We extracted eigenfrequencies and eigenfunctions by applying Fourier transforms on the obtained time-series. The agreement with literature values is excellent for both non-axisymmetric perturbations of uniformly rotating stars and axisymmetric perturbations of differentially rotating stars.

Our simulations show that a small degree of differential rotation causes the ratio of the critical $T/|W|$, where the f-mode becomes CFS unstable, to the value of $T/|W|$ at the mass-shedding to decrease. This effect is visible for each considered equation of state and is even stronger for the stiffer ones. It implies that neutron stars can be destabilized by the CFS instability even if their spinning frequency is rather low compared to the Kepler frequency. Furthermore, when moving on to a high degree of differential rotation, the critical curve of any considered sequence exhibits a local maximum which is in agreement with Newtonian findings. Afterwards, the critical value decreases and for the sequences based on the stiffer equations of state it decreases even below the corresponding value for rigid rotation; i. e. the CFS instability may act even earlier than in rigidly rotating stars as long as the star rotates with a sufficiently high degree of differential rotation.

Summarized, we showed that both a small and a high degree of differential rotation plays an important role in the evolution of a neutron star. As explained in the introduction, neutron stars rotate differentially most probably directly after their birth, but may do so also at later times. Whenever differential rotation is present, the CFS instability is a promising candidate for the destabilization of a neutron star which may finally lead to a detectable signal of gravitational waves.

Finally, we performed simulations on r-modes. Our results show a good qualitative agreement to Newtonian results. As in earlier studies which do not rely on the slow rotation approximation, we do not see any trace of a continuous spectrum.

A very important issue related to differential rotation is the freedom to construct neutron star models with much higher values of $T/|W|$. This means that nearly all available equations of state can admit models which can be CFS-unstable which is not the case for uniformly rotating stars. This enhances the probability of having the CFS-instability working in the early phases of the proto-neutron star creation which will be a significant boost in our efforts to detect gravitational waves from isolated neutron stars and via such observations to infer and constrain fundamental neutron

star parameters.

V. ACKNOWLEDGMENTS

It is a pleasure to thank N. Stergioulas for providing his `rns` code for differentially rotating background models and for carefully reading this manuscript, providing valuable suggestions for improving the article. We also thank M. Vavoulidis, who found an advantageous formulation of the evolution equations and K. Glampedakis for useful comments. This work was supported by the Deutsche Forschungsgemeinschaft DFG (German Research Foundation) via SFB/TR7, EG was funded by EGO via the VESF fellowship program.

-
- [1] S. Chandrasekhar, *ApJ* **161**, 561 (1970).
 - [2] J. L. Friedman and B. F. Schutz, *ApJ* **221**, 937 (1978).
 - [3] J. L. Friedman and B. F. Schutz, *ApJ* **222**, 281 (1978).
 - [4] H. Dimmelmeier, J. A. Font, and E. Müller, *A&A* **393**, 523 (2002).
 - [5] C. D. Ott, A. Burrows, E. Livne, and R. Walder, *ApJ* **600**, 834 (2004).
 - [6] F. A. Rasio and S. L. Shapiro, *ApJ* **432**, 242 (1994).
 - [7] M. Shibata and K. Uryu, *Phys. Rev. D* **61**, 064001 (2000).
 - [8] F. A. Rasio and S. L. Shapiro, *Class. Quantum Gravity* **16**, 1 (1999).
 - [9] L. Rezzolla, F. K. Lamb, and S. L. Shapiro, *ApJ* **531**, L139 (2000).
 - [10] Y. Levin and G. Ushomirsky, *MNRAS* **324**, 917 (2001).
 - [11] N. Stergioulas and J. A. Font, *Phys. Rev. Lett.* **86**, 1148 (2001).
 - [12] P. M. Sá, *Phys. Rev. D* **69**, 084001 (2004).
 - [13] S. L. Shapiro, *ApJ* **544**, 397 (2000).
 - [14] J. N. Cook, S. L. Shapiro, and B. C. Stephens, *ApJ* **599**, 1272 (2003).
 - [15] D. J. Hegyi, *ApJ* **217**, 244 (1977).
 - [16] Y. T. Liu and S. L. Shapiro, *Phys. Rev. D* **69**, 044009 (2004).
 - [17] S. Karino and Y. Eriguchi, *ApJ* **578**, 413 (2002).
 - [18] A. Stavridis, A. Passamonti, and K. Kokkotas, *Phys. Rev. D* **75**, 064019 (2007).
 - [19] A. Passamonti, A. Stavridis, and K. D. Kokkotas, *Phys. Rev. D* **77**, 024029 (2008).
 - [20] N. Stergioulas, T. A. Apostolatos, and J. A. Font, *MNRAS* **352**, 1089 (2004).
 - [21] H. Dimmelmeier, N. Stergioulas, and J. A. Font, *MNRAS* **368**, 1609 (2006).
 - [22] S. Yoshida, L. Rezzolla, S. Karino, and Y. Eriguchi, *ApJ* **568**, L41 (2002).
 - [23] M. Shibata, S. Karino, and Y. Eriguchi, *MNRAS* **334**, L27 (2002).
 - [24] M. Shibata and Y.-I. Sekiguchi, *Phys. Rev. D* **71**, 024014 (2005).
 - [25] J. M. Centrella, K. C. B. New, L. L. Lowe, and J. D. Brown, *ApJ* **550**, L193 (2001).
 - [26] M. Saijo, T. W. Baumgarte, and S. L. Shapiro, *ApJ* **595**, 352 (2003).
 - [27] S. Ou and J. E. Tohline, *ApJ* **651**, 1068 (2006).
 - [28] A. L. Watts, N. Andersson, and D. I. Jones, *ApJ* **618**, L37 (2005).
 - [29] M. Saijo and S. Yoshida, *MNRAS* **368**, 1429 (2006).
 - [30] H. Komatsu, Y. Eriguchi, and I. Hachisu, *MNRAS* **237**, 355 (1989).
 - [31] H. Komatsu, Y. Eriguchi, and I. Hachisu, *MNRAS* **239**, 153 (1989).
 - [32] K. D. Kokkotas and M. Vavoulidis, *JPCS* **8**, 71 (2005).
 - [33] M. Vavoulidis, Ph.D. Thesis, Aristotle University of Thessaloniki (2007).
 - [34] K. H. Lockitch and J. L. Friedman, *ApJ* **521**, 764 (1999).
 - [35] A. Stavridis and K. D. Kokkotas, *Int. J. Mod. Phys.* **14**, 543 (2005).
 - [36] N. Stergioulas (1995), URL <http://www.gravity.phys.uwm.edu/rns/>.
 - [37] N. Stergioulas and J. L. Friedman, *ApJ* **444**, 306 (1995).
 - [38] E. Gaertig and K. D. Kokkotas, *Phys. Rev. D* **78**, 064063 (2008).
 - [39] E. Gaertig and K. D. Kokkotas, *Phys. Rev. D* **80**, 064026 (2009).
 - [40] F. Ozel, *Nature* **441**, 1115 (2006).
 - [41] F. Ozel, T. Guver, and D. Psaltis, *ApJ* **693**, 1775 (2009).
 - [42] H. Sotani and K. D. Kokkotas, *Phys. Rev. D* **70**, 084026 (2004).
 - [43] J. Diaz Alonso and J. M. Ibanez Cabanell, *ApJ* **291**, 308 (1985).
 - [44] W. D. Arnett and R. L. Bowers, *ApJS* **33**, 415 (1977).
 - [45] H.-O. K. Bertil Gustafsson and J. Olinger, *Time Dependent Problems and Difference Methods* (John Wiley & Sons, 1996).
 - [46] W. Kastaun, *Phys. Rev. D* **77**, 124019 (2008).
 - [47] C. Krüger, Diploma Thesis, Eberhard-Karls University of Tübingen (2009).
 - [48] B. Zink, private communication.

- [49] T. W. Baumgarte, S. L. Shapiro, and M. Shibata, *ApJ* **528**, L29 (2000).
- [50] N. Andersson, *ApJ* **502**, 708 (1998).
- [51] S. Karino, S. Yoshida, and Y. Eriguchi, *Phys. Rev. D* **64**, 024003 (2001).
- [52] S. Yoshida, S. Yoshida, and Y. Eriguchi, *MNRAS* **356**, 217 (2005).
- [53] Y. Kojima, *MNRAS* **293**, 49 (1998).
- [54] H. R. Beyer and K. D. Kokkotas, *MNRAS* **308**, 745 (1999).
- [55] J. Ruoff and K. D. Kokkotas, *MNRAS* **328**, 678 (2001).